Supplement of Biogeosciences, 20, 2251–2263, 2023
https://doi.org/10.5194/bg-20-2251-2023-supplement

Biogeosciences
Open Access

Supplement of

Assessing global-scale organic matter reactivity patterns in marine sediments using a lognormal reactive continuum model

Sinan Xu et al.

Correspondence to: Zijun Wu (wuzj@tongji.edu.cn)

1. Details of investigated sites.

Table S1. Supplementary sources of data for Fig. 3 in the main text.

longitude	latitude	Sea area	Water depth	ω	G_{max}	Ref.
(°)	(°)	(Ocean)	(*m*)	(*cm/a*)	(*wt%*)	
72°45′ W	42°15′ N	Long Island Sound	10	0.2	1.7	(1)
131°75′ E	43°11′ N	Amur Bay	1	0.3	2.9	(29)
130°72′ E	42°61′ N	Ekspeditsii Bight	1.5	0.4	2.1	(29)
131°83′ E	42°96′ N	Voevoda bight	2.1	0.3	6.2	(29)
09°08′ E	56°53.10′ N	Livø Strait	7	0.1	6.2	(27)
04°18′ E	51°77′ N	Haringvliet Lake	7.5	1.01	4.73	(26)
123°29′ W	48°36′ N	NorthCarolina,USA	8	0.15	4.5	(9)
09°09′ E	56°50.32′ N	Bjørnsholm Bay	10	0.1	12	(27)
70°63′ W	41°73.8′ N	Buzzards Bay	15	0.2	1.9	(14)
70°62′ W	41°74.4′ N	Buzzards Bay	16	0.2	2.1	(14)
71°41′ W	41°43.9′ N	Rhode Island	17	0.2	16	(14)
89°44′ W	29°07′ N	Mississippi River	20	0.8	0.9	(22)
89°35′ W	29°06′ N	Mississippi River	20	0.8	0.52	(22)
73°42′ W	43°81′ S	Southern Chilean	20	0.29	1.4	(23)
73°51′ W	43°47′ S	Southern Chilean	20	0.29	3.2	(23)
73°63′ W	44°62′ S	Southern Chilean	20	0.29	3.1	(23)
73°18′ W	45°31′ S	Southern Chilean	20	0.29	1.6	(23)
74°46′ W	44°51′ S	Southern Chilean	20	0.29	2.4	(23)
74°53′ W	45°68′ S	Southern Chilean	20	0.29	1.5	(23)
13°86′ E	54°74′ N	Arkona Bassin	35	0.048	3.8	(21)
13°79′ E	54°80′ N	Arkona Bassin	44	0.074	4.1	(21)
13°66′ E	54°94′ N	Arkona Bassin	44	0.19	5.2	(21)
13°61′ E	54°91′ N	Arkona Bassin	44	0.215	4.9	(21)
136°78′ W	34°29′ N	Ago Bay	50	0.2	2.5	(18)
136°72′ W	34°30′ N	Ago Bay	50	0.2	2.4	(18)
136°70′ W	34°25′ N	Ago Bay	50	0.2	2.48	(18)
14°18′ E	23°46.52′ S	Namibian shelf	110	0.34	12	(16)
86°13′ W	09°37′ N	Costa Rica	160	0.01	2.4	(20)
86°11′ W	09°39′ N	Costa Rica	160	0.01	1.75	(20)
86°15′ W	09°42′ N	Costa Rica	160	0.01	1.6	(20)
123°25′ W	48°32′ N	Saanich Inlet	170	0.69	4.8	(7)
05°12′ W	78°93′ N	East Greenland shelf	189	0.37	0.72	(24)
12°77′ W	74°99′ N	East Greenland shelf	320	0.46	0.48	(24)
04°59′ W	75°06′ N	Central Greenland	272	0.09	0.62	(24)
123°30′ W	48°37′ N	Saanich Inlet	210	1.04	3.8	(11)
77°39′ W	12°0.5′ S	Peru continental	186	0.23	14	(2)
77°40′ W	12°0.5′ S	Peru continental	255	0.23	7.9	(2)
76°50′ W	13°37.3′ S	Peru continental	370	0.14	20	(5)
76°51′ W	13°37.3′ S	Peru continental	370	0.04	20	(5)
77°57′ W	11°15.1′ S	Peru continental	186	0.15	14	(5)

78°07′ W	11°20.6′ S	Peru continental	411	0.15	20	(4)
77°24′ W	12°23′ S	Peruvian margin	297	0.06	17.2	(33)
77°10′ W	12°13′ S	Peruvian margin	306	0.3	3.1	(33)
77°15′ W	12°17′ S	Peruvian margin	409	0.5	14.8	(33)
24°59′ W	71°21′ N	Weddell Sea	422	0.58	0.28	(25)
120°14′ W	34°19.3′ N	Santa Barbara Basin	430	0.2	2.8	(13)
120°01′ W	34°14.3′ N	Santa Barbara Basin	578	0.2	3.2	(13)
120°02′ W	34°16.0′ N	Santa Barbara Basin	585	0.2	2.6	(13)
12°85′ E	38°13′ N	Castellammare	550	0.2	1.1	(28)
12°91′ E	38°14′ N	Castellammare	550	0.2	0.85	(28)
146°00′ E	49°44.88′ N	Sea of Okhotsk	613	0.093	2.1	(30)
144°04′ E	54°26.52′ N	Sea of Okhotsk	685	0.022	1.7	(30)
144°42′ E	52°43.88′ N	Sea of Okhotsk	713	0.115	1.8	(30)
144°14′ E	53°50.00′ N	Sea of Okhotsk	771	0.092	1.7	(30)
146°02′ E	48°22.73′ N	Sea of Okhotsk	1256	0.013	1.6	(30)
146°08′ E	48°11.83′ N	Sea of Okhotsk	1602	0.01	0.83	(30)
77°11′ W	12°14′ S	Peruvian margin	695	0.3	6.1	(33)
77°35′ W	12°31′ S	Peruvian margin	756	0.08	2.9	(33)
77°40′ W	12°35′ S	Peruvian margin	770	0.052	4.6	(33)
02°45′ W	62°79′ N	Shetland Faeroe	777	0.68	1.2	(24)
119°42′ E	22°29′ N	South China Sea	1004	0.08	0.78	(32)
38°51′ W	77°39′ N	Weddell Sea	1097	0.21	0.42	(25)
31°24′ W	74°24′ N	Weddell Sea	1178	0.14	0.36	(25)
09°67′ W	68°71′ N	Weddell Sea	1185	0.08	0.32	(25)
27°64′ W	73°17′ N	Weddell Sea	1566	0.24	0.35	(25)
22°36′ W	73°36′ N	Weddell Sea	1598	0.24	0.25	(25)
27°16′ W	73°48′ N	Weddell Sea	444	0.74	0.21	(25)
118°83′ W	32°85′ N	Southern California	1500	0.06	6.5	(23)
65°35′ E	20°00′ N	Arabian Sea	3000	0.0024	0.56	(31)
68°33′ E	15°36′ N	Arabian Sea	3500	0.0025	0.95	(31)
64°33′ E	14°24′ N	Arabian Sea	3500	0.0024	0.63	(31)
65°02′ E	10°03′ N	Arabian Sea	3500	0.0012	0.53	(31)
60°31′ E	16°10′ N	Arabian Sea	4000	0.0034	3.8	(31)
71°24′ W	36°10′ N	NW Atlantic	4215	0.01	1.2	(8)
70°50′ W	32°59.3′ N	NW Atlantic	4595	0.003	0.28	(8)
60°50′ W	35°19.8′ N	NW Atlantic	5341	0.01	0.34	(8)
136°03′ E	28°59.00′ N	Philippine Sea	2972	0.00006	0.34	(6)
135°93′ E	29°08.00′ N	Shikoku Basin	2972	0.00006	0.5	(6)
135°99′ E	29°10.00′ N	Shikoku Basin	2972	0.00006	0.42	(6)
134°93′ E	28°59.00′ N	Shikoku Basin	2972	0.00002	0.27	(6)
151°39′ W	13°41.7′ N	the North Pacific	5686	0.00015	0.4	(10)
148°57′ W	6°13.2′ N	the North Pacific	5718	0.00019	0.23	(10)
146°09′ W	9°30.5′ N	the North Pacific	5004	0.00023	0.36	(10)
146°01′ W	9°19.3′ N	the North Pacific	5205	0.00032	0.45	(10)

145°59′ W	9°31.5′ N	the North Pacific	5164	0.00036	0.26	(10)
144°49′ W	3°59.5′ N	the North Pacific	5214	0.00036	0.22	(10)
145°01′ W	3°50.2′ N	the North Pacific	4599	0.00041	0.23	(10)
148°44′ W	9°15.0′ N	the North Pacific	4619	0.00043	0.35	(10)
148°46′ W	9°06.5′ N	the North Pacific	5144	0.00058	0.32	(10)
151°39′ W	14°41.7′ N	the North Pacific	5686	0.0002	0.2	(10)
148°47′ W	9°06.5′ N	the North Pacific	5189	0.0012	0.25	(10)
168°46′ W	65°01.7′ S	South flank Pacific	2930	0.00258	0.5	(12)
174°14′ W	66°49.7′ S	South flank Pacific	3260	0.0018	0.32	(12)
174°44′ W	62°54.2′ S	North flank Pacific	4139	0.00588	0.6	(12)
63°27′ W	22°54.9′ N	Nares Abyssal Plain	5868	0.0005	0.3	(15)
63°26′ W	22°54.9′ N	Nares Abyssal Plain	5868	0.0005	0.14	(15)
63°00′ W	23°22.3′ N	Nares Abyssal Plain	5878	0.0005	0.12	(15)
63°01′ W	23°22.3′ N	Nares Abyssal Plain	5878	0.0005	0.008	(15)
169°04′ E	08°13′ N	Equatorial Pacific	4239	<0.002	0.25	(17)
177°58′ E	07°27′ N	Equatorial Pacific	5269	<0.002	0.42	(17)
175°52′ W	05°03′ N	Equatorial Pacific	5867	<0.002	0.6	(17)
174°54′ W	03°04′ N	Equatorial Pacific	3572	<0.002	0.54	(17)
171°04′ W	00°02′ S	Equatorial Pacific	5352	<0.002	0.7	(17)
168°04′ W	02°26′ S	Equatorial Pacific	5361	<0.002	0.52	(17)
166°37′ W	03°39′ S	Equatorial Pacific	5469	<0.002	0.53	(17)
166°32′ W	09°10′ S	Equatorial Pacific	5283	<0.002	0.15	(17)
85°22′ W	05°30′ S	Peru Basin	4082	0.002	1.7	(19)
85°11′ W	06°34′ S	Peru Basin	4165	0.0006	0.72	(19)
88°27′ W	07°40′ S	Peru Basin	4127	0.0004	0.8	(19)
3.07 W	51.5 N	Severn estuary	8	0.43	2.9	(34)
4.85 E	43.31 N	Rhone zone	19	0.1	1.9	(35)
4.77 E	43.27 N	Rhone shelf	74	0.5	1.5	(36)
10.34 E	56.11 N	Aarhus Bay	15	0.32	3.8	(37)
13.78 E	54.8 N	Arkona Basin	43	0.0074	3.9	(38)
7.97 E	54.08 N	Helgoland Mud	29	1.3	1.1	(39)
9.75 E	57.92 N	Skagerrak S10	86	0.5	1.4	(40)
9.7 E	57.95 N	Skagerrak S11	150	0.5	0.7	(41)
9.6 E	58.05 N	Skagerrak S13	386	0.5	2.1	(42)
63.02 E	24.88 N	Arabian Sea	645	0.05	1.1	(43)
62.99 E	24.81 N	Arabian Sea	957	0.05	0.95	(44)
62.99 E	24.71 N	Arabian Sea	1586	0.05	0.92	(45)
168.8 W	54.57 N	Bering Sea	1476	0.0016	1.6	(46)
53.59 W	39.31 S	Argentine Basin	3687	0.008	1.2	(47)

Reference for supplementary Table 4

[1] Goldhaber, M. B., Aller, R. C., Cochran, J. K., Rosenfeld, J. K., Martens, C. S., & Berner, R. A. (1977). Sulfate reduction, diffusion, and bioturbation in Long Island Sound sediments; report of the FOAM Group. American Journal of Science, 277(3), 193-237.

[2] Froelich, P. N., Arthur, M. A., Burnett, W. C., Deakin, M., Hensley, V., Jahnke, R., ... & Vathakanon, C. (1988). Early diagenesis of organic matter in Peru continental margin sediments: phosphorite precipitation. Marine Geology, 80(3-4), 309-343.

[3] Müller, P. J., & Mangini, A. (1980). Organic carbon decomposition rates in sediments of the Pacific manganese nodule belt dated by 230Th and 231Pa. Earth and planetary science letters, 51(1), 94-114.

[4] Reimers, C. E. (1982). Organic matter in anoxic sediments off central Peru: relations of porosity, microbial decomposition and deformation properties. Marine Geology, 46(3-4), 175-197.

[5] Reimers, C. E., & Suess, E. (1983). The partitioning of organic carbon fluxes and sedimentary organic matter decomposition rates in the ocean. Marine Chemistry, 13(2), 141-168.

[6] Waples, D. W., & Sloan, J. R. (1980). Carbon and nitrogen diagenesis in deep sea sediments. Geochimica et Cosmochimica Acta, 44(10), 1463-1470.

[7] Hamilton, S. E., & Hedges, J. I. (1988). The comparative geochemistries of lignins and carbohydrates in an anoxic fjord. Geochimica et Cosmochimica Acta, 52(1), 129-142.

[8] Heggie, D., Maris, C., Hudson, A., Dymond, J., Beach, R., & Cullen, J. (1987). Organic carbon oxidation and preservation in NW Atlantic continental margin sediments. Geological Society, London, Special Publications, 31(1), 215-236.

[9] Martens, C. S., & Klump, J. V. (1984). Biogeochemical cycling in an organic-rich coastal marine basin 4. An organic carbon budget for sediments dominated by sulfate reduction and methanogenesis. Geochimica et Cosmochimica Acta, 48(10), 1987-2004.

[10] Müller, P. J., & Mangini, A. (1980). Organic carbon decomposition rates in sediments of the Pacific manganese nodule belt dated by 230Th and 231Pa. Earth and planetary science letters, 51(1), 94-114.

[11] Murray, J. W., Grundmanis, V., & Smethie Jr, W. M. (1978). Interstitial water chemistry in the sediments of Saanich Inlet. Geochimica et Cosmochimica Acta, 42(7), 1011-1026.

[12] Reimers, C. E., & Suess, E. (1983). The partitioning of organic carbon fluxes and sedimentary organic matter decomposition rates in the ocean. Marine Chemistry, 13(2), 141-168.

[13] Sholkovitz, E. (1973). Interstitial water chemistry of the Santa Barbara Basin sediments. Geochimica et Cosmochimica Acta, 37(9), 2043-2073.

[14] Henrichs, S. M., & Farrington, J. W. (1987). Early diagenesis of amino acids and organic matter in two coastal marine sediments. Geochimica et Cosmochimica Acta, 51(1), 1-15.

[15] Thomson, J., Higgs, N. C., & Colley, S. (1989). A geochemical investigation of reduction haloes developed under turbidites in brown clay. Marine geology, 89(3-4), 315-330.

[16] Dale, A. W., Brüchert, V., Alperin, M., & Regnier, P. (2009). An integrated sulfur isotope model for Namibian shelf sediments. Geochimica et Cosmochimica Acta, 73(7), 1924-1944.

[17] Grundmanis, V., & Murray, J. W. (1982). Aerobic respiration in pelagic marine sediments. Geochimica et Cosmochimica Acta, 46(6), 1101-1120.

[18] Kasih, G. A., Chiba, S., Yamagata, Y., Shimizu, Y., & Haraguchi, K. (2008). Modeling early diagenesis of sediment in Ago Bay, Japan: A comparison of steady state and dynamic calculations. Ecological modelling, 215(1-3), 40-54.

[19] Haeckel, M., König, I., Riech, V., Weber, M. E., & Suess, E. (2001). Pore water profiles and numerical modelling of biogeochemical processes in Peru Basin deep-sea sediments. Deep Sea Research Part II: Topical Studies in Oceanography, 48(17-18), 3713-3736.

[20] Hensen, C., & Wallmann, K. (2005). Methane formation at Costa Rica continental margin—

constraints for gas hydrate inventories and cross-décollement fluid flow. Earth and Planetary Science Letters, 236(1-2), 41-60.
[21] Mogollón, J. M., Dale, A. W., Fossing, H., & Regnier, P. (2012). Timescales for the development of methanogenesis and free gas layers in recently-deposited sediments of Arkona Basin (Baltic Sea). Biogeosciences (BG), 9, 1915-1933.
[22] Morse, J. W., & Eldridge, P. M. (2007). A non-steady state diagenetic model for changes in sediment biogeochemistry in response to seasonally hypoxic/anoxic conditions in the "dead zone" of the Louisiana shelf. Marine Chemistry, 106(1-2), 239-255.
[23] Rojas, N., & Silva, N. (2005). Early diagenesis and vertical distribution of organic carbon and total nitrogen in recent sediments from southern Chilean fjords (Boca del Guafo to Pulluche Channel). Investigaciones marinas, 33(2), 183-194.
[24] Sauter, E. J., Schlüter, M., & Suess, E. (2001). Organic carbon flux and remineralization in surface sediments from the northern North Atlantic derived from pore-water oxygen microprofiles. Deep Sea Research Part I: Oceanographic Research Papers, 48(2), 529-553.
[25] Schlüter, M. (1991). Organic carbon flux and oxygen penetration into sediments of the Weddell Sea: indicators for regional differences in export production. Marine chemistry, 35(1-4), 569-579.
[26] Canavan, R. W., Slomp, C. P., Jourabchi, P., Van Cappellen, P., Laverman, A. M., & Van den Berg, G. A. (2006). Organic matter mineralization in sediment of a coastal freshwater lake and response to salinization. Geochimica et Cosmochimica Acta, 70(11), 2836-2855.
[27] Jørgensen, B. B., JØrgensen, B. B., & Parkes, R. J. (2010). Role of sulfate reduction and methane production by organic carbon degradation in eutrophic fjord sediments (Limfjorden, Denmark). Limnology and Oceanography, 55(3), 1338-1352.
[28] Paradis, S., Pusceddu, A., Masqué, P., Puig, P., Moccia, D., Russo, T., & Iacono, C. L. (2019). Organic matter contents and degradation in a highly trawled area during fresh particle inputs (Gulf of Castellammare, southwestern Mediterranean).
[29] Tishchenko, P. Y., Medvedev, E. V., Barabanshchikov, Y. A., Pavlova, G. Y., Sagalaev, S. G., Tishchenko, P. P., ... & Orekhova, N. A. (2020). Organic Carbon and Carbonate System in the Bottom Sediments of Shallow Bights of the Peter the Great Bay (Sea of Japan). Geochemistry International, 58(6), 704-718.
[30] Wallmann, K., Aloisi, G., Haeckel, M., Obzhirov, A., Pavlova, G., & Tishchenko, P. (2006). Kinetics of organic matter degradation, microbial methane generation, and gas hydrate formation in anoxic marine sediments. Geochimica et Cosmochimica Acta, 70(15), 3905-3927.
[31] Luff, R., Wallmann, K., Grandel, S., & Schlüter, M. (2000). Numerical modeling of benthic processes in the deep Arabian Sea. Deep Sea Research Part II: Topical Studies in Oceanography, 47(14), 3039-3072.
[32] Chuang, P. C., Yang, T. F., Wallmann, K., Matsumoto, R., Hu, C. Y., Chen, H. W., ... & Dale, A. W. (2019). Carbon isotope exchange during anaerobic oxidation of methane (AOM) in sediments of the northeastern South China Sea. Geochimica et Cosmochimica Acta, 246, 138-155.
[33] Dale, A. W., Sommer, S., Lomnitz, U., Montes, I., Treude, T., Liebetrau, V., ... & Bryant, L. D. (2015). Organic carbon production, mineralization and preservation on the Peruvian margin. Biogeosciences (BG), 12, 1537-1559.
[34] Langston, W. J., Pope, N. D., Jonas, P. J. C., Nikitic, C., Field, M. D. R., Dowell, B., ... & Brown, A. R. (2010). Contaminants in fine sediments and their consequences for biota of the Severn Estuary. Marine Pollution Bulletin, 61(1-3), 68-82.

[35] Pastor, L., Deflandre, B., Viollier, E., Cathalot, C., Metzger, E., Rabouille, C., ... & Grémare, A. (2011). Influence of the organic matter composition on benthic oxygen demand in the Rhône River prodelta (NW Mediterranean Sea). Continental Shelf Research, 31(9), 1008-1019.
[36] Aquilina, A., Knab, N. J., Knittel, K., Kaur, G., Geissler, A., Kelly, S. P., ... & Pancost, R. D. (2010). Biomarker indicators for anaerobic oxidizers of methane in brackish-marine sediments with diffusive methane fluxes. Organic Geochemistry, 41(4), 414-426.
[37] Thingstad, T. F., Riemann, B. O., Havskum, H., & Garde, K. (1996). Incorporation rates and biomass content of C and P in phytoplankton and bacteria in the Bay of Aarhus (Denmark) June 1992. Journal of plankton research, 18(1), 97-121.
[38] Fleming, V., & Kaitala, S. (2006). Phytoplankton spring bloom intensity index for the Baltic Sea estimated for the years 1992 to 2004. Hydrobiologia, 554(1), 57-65.
[39] Hebbeln, D., Scheurle, C., & Lamy, F. (2003). Depositional history of the Helgoland mud area, German Bight, North Sea. Geo-Marine Letters, 23(2), 81-90.
[40] Dahl, E., & Johannessen, T. (1998). Temporal and spatial variability of phytoplankton and chlorophyll a: lessons from the south coast of Norway and the Skagerrak. ICES Journal of Marine Science, 55(4), 680-687.
[41] Richardson, K., Rasmussen, B., Bunk, T., & Mouritsen, L. T. (2003). Multiple subsurface phytoplankton blooms occurring simultaneously in the Skagerrak. Journal of plankton research, 25(7), 799-813.
[42] Trimmer, M., Engström, P., & Thamdrup, B. (2013). Stark contrast in denitrification and anammox across the deep Norwegian trench in the Skagerrak. Applied and environmental microbiology, 79(23), 7381-7389.
[43] Bard, E., Ménot, G., Rostek, F., Licari, L., Böning, P., Edwards, R. L., ... & Heaton, T. J. (2013). Radiocarbon calibration/comparison records based on marine sediments from the Pakistan and Iberian margins. Radiocarbon, 55(4), 1999-2019.
[44] Barlow, R. G., Mantoura, R. F. C., & Cummings, D. G. (1999). Monsoonal influence on the distribution of phytoplankton pigments in the Arabian Sea. Deep Sea Research Part II: Topical Studies in Oceanography, 46(3-4), 677-699.
[45] Koho, K. A., Nierop, K. G. J., Moodley, L., Middelburg, J. J., Pozzato, L., Soetaert, K., ... & Reichart, G. J. (2013). Microbial bioavailability regulates organic matter preservation in marine sediments. Biogeosciences, 10, 1131-1141.
[46] Coyle, K. O., Pinchuk, A. I., Eisner, L. B., & Napp, J. M. (2008). Zooplankton species composition, abundance and biomass on the eastern Bering Sea shelf during summer: the potential role of water-column stability and nutrients in structuring the zooplankton community. Deep Sea Research Part II: Topical Studies in Oceanography, 55(16-17), 1775-1791.
[47] Benthien, A., & Müller, P. J. (2000). Anomalously low alkenone temperatures caused by lateral particle and sediment transport in the Malvinas Current region, western Argentine Basin. Deep Sea Research Part I: Oceanographic Research Papers, 47(12), 2369-2393.

2. Parameter sensitivity analysis for the *l*-RCM and the *γ*-RCM

We did parameter sensitivity analysis for *γ*-RCM and *l*-RCM, respectively. The results shown that when v is fixed value, the parameter a can vary over a wide range (from 10000 to 20000) while maintaining a relatively good fit (R^2>0.9). However, when a is a fixed value, the variation of parameter v can cause a large fitting error. The results were shown in the Table S2 and Fig. S1.

Besides, we found when both *a* and *v* had a huge change, *γ*-RCM can also obtain a good fit result, as shown in the Fig. S3.

Table S2. Fitting results of parametric sensitivity analysis of *γ*-RCM

Sensitivity analysis of *γ*-RCM							
BX-6	***v*=0.278**	*a*=12.5	R^2=0.82	**DSDP 58**	***v*=1.08**	*a*=10224	R^2=0.91
		a=22.5	R^2=0.93			*a*=12224	R^2=0.92
		a=32.5	R^2=0.86			*a*=14224	R^2=0.93
		a=42.5	R^2=0.74			*a*=16224	R^2=0.92
		a=52.5	R^2=0.61			*a*=18224	R^2=0.92
						a=20224	R^2=0.92
	***a*=22.5**	*v*=0.178	R^2=0.56		***a*=20224**	*v*=0.68	R^2=0.63
		v=0.278	R^2=0.93			*v*=0.88	R^2=0.84
		v=0.378	R^2=0.76			*v*=1.08	R^2=0.92
						v=1.28	R^2=0.93
						v=1.48	R^2=0.91

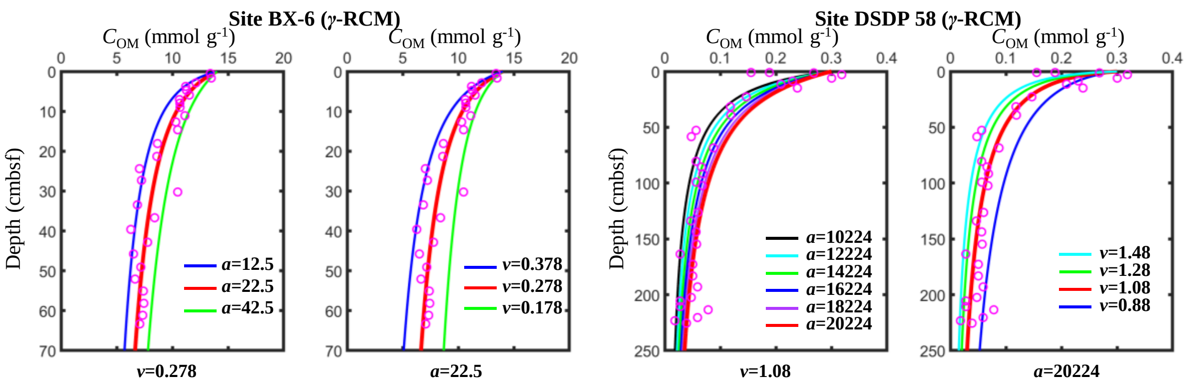

Fig. S1. Parameter sensitivity analysis of *γ*-RCM.

The *l*-RCM best-fit parameters are well fixed. According to the parametric sensitivity analysis, we found that very small changes in parameters *μ* and *σ* can cause large errors in the fitting results. The results were shown in the Table S3 and Fig. S2.

Table S3. Fitting results of parametric sensitivity analysis of *l*-RCM.

Sensitivity analysis of *l*-RCM							
BX-6	***μ*=2.24 ×10^{-3}**	*σ*=1.031	R^2=0.71	**DSDP 58**	***μ*=6.11 ×10^{-5}**	*σ*=0.663	R^2=0.87
		σ=2.031	R^2=0.93			*σ*=1.663	R^2=0.92
		σ=3.031	R^2=0.88			*σ*=2.663	R^2=0.88
		σ=4.031	R^2=0.83			*σ*=3.663	R^2=0.81
	***σ*=2.031**	$\mu=1.24\times10^{-3}$	R^2=0.62		***σ*=1.663**	$\mu=3.11\times10^{-5}$	R^2=0.86
		$\mu=2.24\times10^{-3}$	R^2=0.93			$\mu=6.11\times10^{-5}$	R^2=0.92
		$\mu=3.24\times10^{-3}$	R^2=0.89			$\mu=9.11\times10^{-5}$	R^2=0.87
		$\mu=4.24\times10^{-3}$	R^2=0.82			$\mu=12.11\times10^{-5}$	R^2=0.82

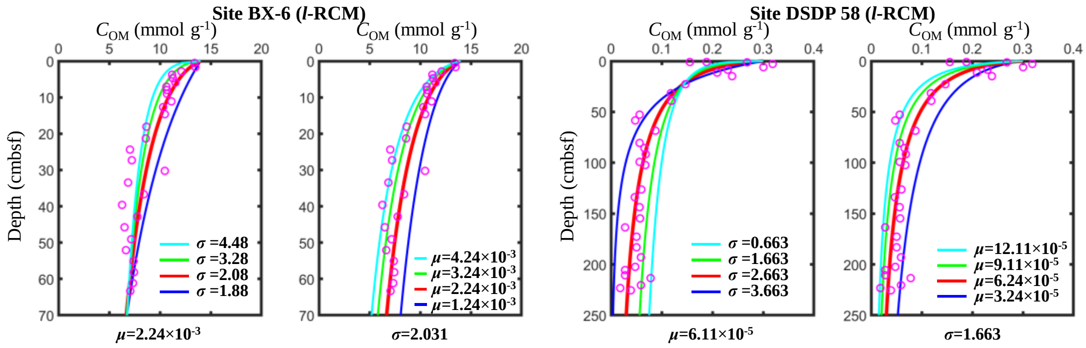

Fig. S2. Parameter sensitivity analysis of *l*-RCM.

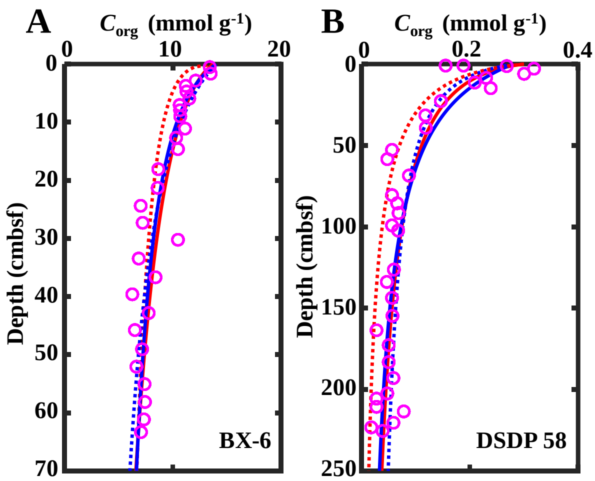

Fig. S3. A: pink circles are measured OM date. The red solid (μ=2.23×10^{-3}, σ=2.03, R^2=0.93) and dotted lines (μ=2.23×10^{-3}, σ=1.03, R^2=0.82) are the results of *l*-RCM, the blue solid (v=0.278, a=22.5, R^2=0.93) and dotted lines (v=0.5, a=53, R^2=0.91) are the results of γ-RCM. B: pink circles are measured OM date. The red solid (μ=6.11×10^{-5}, σ=1.66, R^2=0.92) and dotted lines (μ=8.8×10^{-5}, σ=1.36, R^2=0.78) are the results of *l*-RCM, the blue solid (v=1.08, a=20225, R^2=0.92) and dotted lines (v=0.5, a=4024, R^2=0.89) are the results of γ-RCM.